Chaos, Solitons and Fractals 162 (2022) 112410

Contents lists available at ScienceDirect

Chaos, Solitons and Fractals

Nonlinear Science, and Nonequilibrium and Complex Phenomena

journal homepage: www.elsevier.com/locate/chaos

Break-up of invariant curves in the Fermi-Ulam model

Joelson D.V. Hermes [a,b,*], Marcelo A. dos Reis [a,c], Iberê L. Caldas [d], Edson D. Leonel [b]

[a] Federal Institute of Education, Science and Technology of South of Minas Gerais - IFSULDEMINAS, Inconfidentes, Brazil
[b] Departamento de Física, Universidade Estadual Paulista (UNESP), Campus Rio Claro, Av. 24A, 1515, 13506-900, SP, Brazil
[c] Escola Preparatória de Cadetes do Exército - EsPCEx, Campinas, SP, Brazil
[d] Physics Institute, University of São Paulo, São Paulo, SP, Brazil

ARTICLE INFO

Article history:
Received 11 February 2022
Received in revised form 27 June 2022
Accepted 1 July 2022
Available online xxxx

Keywords:
Chaos
Nonlinear dynamics
Mappings
Hamiltonian systems

ABSTRACT

The transport of particles in the phase space is investigated in the Fermi-Ulam model. The system consists of a particle confined to move within two rigid walls with which it collides. One is fixed and the other is periodically moving in time. In this work we investigate, for this model, the location of invariant curves that separate chaotic areas in the phase space. Applying the Slater's theorem we verify that the mapping presents a family of invariant spanning curves with a rotation number whose expansion into continued fractions has an infinite tail of the unity, acting as local transport barriers. We study the destruction of such curves and find the critical parameters for that. The determination of the rotation number in the vicinity of one of the considered spanning curves allowed us to understand the dynamics in the vicinity of the considered curve, both before and after criticality. The rotation number profile showed us the fractal character of the region close to the curve, since this profile has a structure similar to a "Devil's Staircase".

1. Introduction

The study of two-dimensional Hamiltonian systems connects several areas, due to the capacity of the Hamiltonian formalism to describe a great diversity of models. This formalism is applied to channel flows [1,2], transport properties [3–5], magnetic field lines [6,7], waveguides [8,9], Fermi acceleration [10,11] among others [12,13]. An important part of the study of Hamiltonians, for quasi-integrable systems, is associated to the called KAM theorem (stated by Kolmogorov, demonstrated for flows by Arnold and for maps by Moser) [14–17]. This theorem guarantees the persistence of some invariant tori (invariant curves) for quasi-integrable maps, eventually, these invariant tori are destroyed by sufficiently large perturbations. However, for small perturbation values, some of these tori persist and act as transport barriers [18], in addition to limiting the size of the chaotic sea. In these circumstances, these curves play a crucial role in the study of transport properties, diffusion, and scales in the chaotic sea, among other applications.

We investigate the destruction of these curves in the Fermi-Ulam model. This model was initially introduced by Fermi [19] to explain the acceleration of cosmic rays. According to him, charged particles traveling in the interstellar medium would be accelerated by oscillating electromagnetic fields coming from stars and galaxies. Later, based on this proposal, Ulam [20] proposed a model in which a particle would be confined between two rigid walls, colliding between them, one being fixed and the other moving periodically in time. Over the years there has been a wide variety of work involving this model, in which scientists seek to understand and explore its properties, this is due to the relevance this model has in the field of dynamical systems. Among these works, it is worth mentioning [21] where the authors reduced the Fermi problem to a Hamiltonian form and using this technique they estimated the location of absolute barriers in the phase space of the system. However, the determination of these barriers with high precision is still little explored for this model. Works such as [22,23] only confirm the existence of these curves, but do not show their position in phase space nor predict the value of the parameter from which they are destroyed.

Invariant curves are orbits with irrational rotation in phase space and over the circle. In this context, such orbits can be related to Slater's theorem [24]. This theorem states that a translation on a unit circle has at most three different return times and that these times are part of the expansion into continued fractions of the irrational used in the translation. Our purpose is to determine with high precision the location of invariant curves for the Fermi-Ulam model through Slater's theorem and thus understand the behavior of these curves and predict their breakage. For this class of systems, these curves play an essential function regarding the confinement and transport of orbits, since this property is not observed in high-dimensional systems.

* Corresponding author at: Federal Institute of Education, Science and Technology of South of Minas Gerais - IFSULDEMINAS, Inconfidentes, Brazil.
E-mail address: joelson.hermes@rc.unesp.br (J.D.V. Hermes).

https://doi.org/10.1016/j.chaos.2022.112410
0960-0779/

The paper is organized as follow: in Section 2 we present the model as well as some of its properties and make an approximation of the model using the Standard Map as in [25], which allows us to estimate the location of the first invariant spanning curve. In Section 3 we use Slater's theorem, which is based on recurrence times, to determine with high precision the location and destruction of a family of invariant curves. Next, in Section 4, through the rotation number profile we analyze the neighborhood of one of the invariant curves to understand the dynamics in its vicinity and in Section 5 we present our final considerations.

2. The model

The model consists of a classical particle that moves between two walls, one fixed and the other movable. The particle collides elastically with the walls, where it assumes that the walls have infinite mass, such walls allude to the magnetic fields with which the particles collide, as proposed by Fermi. The position of the movable wall is given by $x_w(t) = X_0 \cos(wt)$ where X_0 is the amplitude of the motion and w is the frequency, meanwhile the fixed wall is located at $X = \ell$. In order to avoid the numerical resolution of transcendental equations, which can be very expensive from a computational point of view, we assume that the distance between the walls is fixed, therefore, the version of the model we consider in this paper is the so called static wall approximation [21,26]. This simplified version maintains most of the properties observed in the full version without requiring the solution of the transcendental equations.

The mapping describing the dynamics of the model is written as

$$T: \begin{cases} \phi_{n+1} = \left[\phi_n + \dfrac{2}{V_n}\right] \bmod 2\pi \\ V_{n+1} = \left|V_n - 2\varepsilon \sin(\phi_{n+1})\right|, \end{cases} \tag{1}$$

where we considered a set of dimensionless variables such as $\varepsilon = X_0/\ell$, $V_n = v_n/(w\ell)$ with v_n representing the velocity of the particle and $\phi = wt$. Fixed points for this mapping can be obtained by applying the following conditions: $V_{n+1} = V_n = V$ and $\phi_{n+1} = \phi_n = \phi + 2k\pi$, where $k = 1,2,3, \ldots$ identifies the number of oscillations that the moving wall completes between collisions. Simultaneously applying the conditions for the equilibrium state, we have the following fixed points: $(V,\phi) = (\frac{1}{k\pi}, 0)$ which are hyperbolic and $(V,\phi) = (\frac{1}{k\pi}, \pi)$ which are elliptical as long as the condition is satisfied, these points are highlighted in the Fig. 5(a,b).

In Fig. 1 we show the phase space for this mapping with $\varepsilon = 5 \cdot 10^{-4}$, through which it is possible to notice a mixed structure containing a large sea of chaos coexisting with islands of stability and invariant spanning curves. It is well known in the literature that invariant spanning curves act as barriers preventing a particle in the chaotic region below the curve from evolving to a higher energy region above the curve. Thus, the first invariant spanning curve divides the phase space into two distinct regions, the first, below it, called the global chaos region and the second, above the curve, defined as the local chaos region. This behavior allows us to consider that such a model can be approximated locally by the Standard Map establishing a connection between these two models [27], since for the Standard Map it is already known from both analytical and numerical results that there is a critical parameter related to this type of curve.

However, in the vicinity of the first invariant curve there are other invariant curves and, as we increase the control parameter, these invariant curves (irrational tori) are destroyed until the last invariant curve is broken and the chaos that was local becomes global, so there is a critical value of the parameter from which the curve ceases to exist. In this sense, we reinforce that the comparison of the Fermi-Ulam model with the Standard Map is interesting since for the Standard Map this critical value that defines the transition is already known.

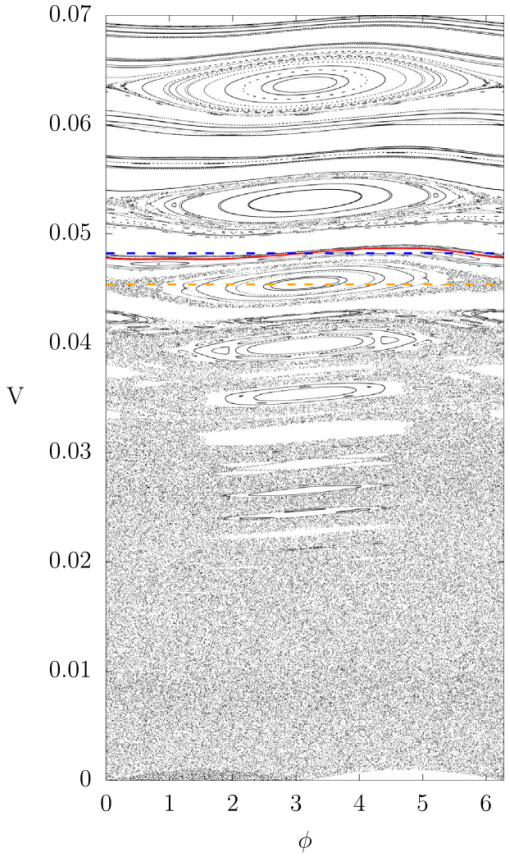

Fig. 1. Phase space for the Fermi-Ulam model given by Eq. (1) with the invariant spanning curve found by the Slater's theorem highlighted in red. The dashed line corresponds to the approximation given by Eq. (2) with $\varepsilon = 5 \cdot 10^{-4}$ (dashed line orange) and with $\varepsilon = \varepsilon_c = 5.652 \cdot 10^{-4}$ (dashed line blue). (For interpretation of the references to colour in this figure legend, the reader is referred to the web version of this article.)

To derive the Standard Map from Eq. (1) we use a linearization close to the first invariant spanning curve as performed in [25,28]. When the second equation of the mapping (1) is written replacing $V_{n+1} = \tilde{V} + \Delta V_{n+1}$ with $\Delta V/\tilde{V} \ll 1$ and Taylor expanding it till first order and that when compared with the equations of the standard mapping leads to

$$\tilde{V} = \frac{2}{\sqrt{0.9716\ldots}}\sqrt{\varepsilon}. \tag{2}$$

This result gives us an approximation of the location of the first invariant spanning curve. We know that the chaotic sea region is confined to the lowest energy domain and limited by the first invariant spanning curve. Therefore, for sufficiently long times, the velocity V approaches a saturation value that depends on the ε parameter, where $V \cong \varepsilon^{\alpha}$, with α being known as the saturation exponent. Through Eq. (2) we have $\alpha = \frac{1}{2}$, in good agreement with numerical results present in the literature [29,30]. However, although this result provides an approximation of the first invariant curve, in the next section we will use a method based on Slater's Theorem that allows us to determine with high precision the position not only of the first invariant curve, but of a family of curves of the type spanning, making it possible to study some dynamic properties of the mapping.

3. The method

Several techniques have been proposed to investigate the behavior of invariant curves, some analytical [31] and others numerical [32–34].

Among them, one that stands out is the method proposed by Greene [34] given its great precision. However, the cited methods present complex mathematics or have numerical implementation difficult and expensive from the computational point of view. Thus, to apply to our model we chose Slater's theorem, as in [35,36]. Its implementation is relatively simple and the computational cost is low. And even so, it allows determining the critical parameter related to a given curve with a known rotation number, giving robust results comparable to Greene's method. Furthermore, through this technique it is possible to determine the position of these curves with high precision, allowing them to be easily located in the phase space.

The theorem shows that for an irrational rotation number ω and for some connected interval there are at most three different return times. Furthermore, in the case of three different return times, the largest one of them is equal to the sum of the other two and yet at least two of them are consecutive denominators in the continued fraction expansion of the irrational number ω,

$$\omega = [a_0; a_1, a_2, a_3, \ldots] \equiv a_0 + \cfrac{1}{a_1 + \cfrac{1}{a_2 + \cfrac{1}{a_3 + \cfrac{1}{\ddots}}}}. \tag{3}$$

Therefore, for an orbit on an invariant curve we will have only three return times and these times will be part of the expansion in continued fractions of the rotation number corresponding to the orbit.

As predicted by KAM theory, invariant curves with suffiently irrational rotation number persist when the perturbation is sufficiently small. Alternatively when the perturbation is large enough, converse KAM theory predicts that there are no invariant curves. Greene [34] conjectured that the last invariant curve for the Chirikov's map has a rotation number equal to the golden mean $\gamma = \frac{1+\sqrt{5}}{2} = [1; 1, 1, 1, \ldots]$. As an example, in Table 1 we show the expansion into continued fractions of the known golden mean γ, as well as some of its convergents $\frac{p_n}{q_n}$. Note that q_n values satisfies the recurrence equation

$$q_n = q_{n-2} + q_{n-1}, \tag{4}$$

for $n = 3, 4, \ldots$ with $q_1 = q_2 = 1$, generating the well-known Fibonacci sequence. So, based on Slater's theorem, the return times for a curve with this rotation number γ are consecutive numbers in the Fibonacci sequence.

John Greene [34] conjectured that the locally more robust invariant curves have a number that is noble. Complementing Greene's theory, Fox [37] showed that invariant curves with noble numbers are locally more robust, even for models other than the Chirikov's map. An irrational number ω is said to be noble if its expansion into continued fractions has a golden mean tail, i.e., it becomes an infinite sequence of 1's at some point, $\omega \equiv [a_0; a_1, a_2, \ldots, a_n, \overline{1}]$. MacKay and Stark presented strong numerical evidence for the robustness of noble invariant curves in [38], where they evidence the robustness of the curve with noble rotation numbers in several generalized standard models. Thus, our proposal is to analyze

Table 1
Representation in continued fractions of the golden mean γ as well as some of its convergents obtained by truncation of the expansions.

n	a_n	Continued Fraction	Convergent
1	1	[1]	1/1
2	1	[1;1]	2/1
3	1	[1;1,1]	3/2
4	1	[1;1,1,1]	5/3
5	1	[1;1,1,1,1]	8/5
6	1	[1;1,1,1,1,1]	13/8
7	1	[1;1,1,1,1,1,1]	21/13
⋮	⋮	⋮	⋮

a family of invariant curves with rotation number of the type $\omega = [a_0; \overline{1}]$ in the Fermi-Ulam Model. Noble numbers of this type are considered the most irrational, in the sense that they are the least easily approximated by rational numbers and, therefore, have a slower convergence in their expansion into continued fractions. Therefore, we believe that curves with these rotation numbers should be more robust, at least locally. Thus, we will determine with high precision the position of each one of these curves in the phase space, as well as study the destruction of than curves and find the critical parameter for those. The Fermi-Ulam Model always presents invariant curves regardless of the value of the parameter ε, but the position of these curves varies accordingly.

The first step to apply the method is to define the rotation number to be investigated. We start our investigation with rotation numbers equal to the golden mean $\gamma = [1; \overline{1}]$ or any shift of this value $\omega = [a_0; \overline{1}]$, because in this way the sequence generated by the denominators of the convergents (q_n) will always be the same and will generate the Fibonacci sequence. Then we set a value of the angular variable $\phi = 3.0$ and vary the value of the action V. For each pair (ϕ_0, V_0) we apply Slater's theorem, that is, we calculate the return time (number of iterations) that the orbit takes to return to an interval δ close to (ϕ_0, V_0). Once these times are calculated, if there are only three distinct times, by Slater's theorem it is possible to conclude that the point (ϕ_0, V_0) is on one invariant curve. Whether, in addition, these three times are consecutive numbers of the Fibonacci sequence, it means that this is the wanted invariant curve. If not, we take a step ΔV in the action variable V and repeat the procedure indicated above, until Slater's theorem is observed and so the pair (ϕ_c, V_c) for which the condition was satisfied belongs to the invariant spanning curve.

In Fig. 1 the curve highlighted in red obeys Slater's theorem and was obtained using the described method. For this curve the return times found were $\Gamma_1 = 75025$, $\Gamma_2 = 121393$ and $\Gamma_3 = 196418$, with recurrence interval $\delta = 10^{-4}$, step $\Delta V = 10^{-13}$ and coordinates $(\phi_c = 3.0, V_c = 0.0481812264816)$. This curve plays an important role in dynamic systems, as it acts as a barrier that limits the chaotic sea below it, preventing an orbit in the chaotic sea from entering the stability region. For comparison, we indicate in orange the approximate last invariant curve obtained by using the approximation given by eq. (2), namely, $\varepsilon = 5 \cdot 10^{-4}$.

The method can still be used to determine the critical parameter ε_c for a given curve, that is, the value of ε from which the curve is destroyed. However, it is worth noting that the position of the curve varies slightly as we change the value of the parameter ε, as the determination of ε_c requires successive applications of the method. Once a point (ϕ_0, V_0) of the curve is determined by the procedure indicated above, we increase the value of ε and repeat the procedure to find the new position of the curve. This procedure is repeated until Slater's theorem prediction is no longer observed. And the last value of ε for which the condition was observed is the critical parameter ε_c for the studied curve. This means that in the vicinity of this curve, the other invariant spanning curves have already been destroyed, leaving only it or a thin layer containing it.

Applying this technique to the curve highlighted in Fig. 1, we find that the critical parameter ε_c for this curve is $\varepsilon_c = 0.0005652$, this means that from this value this curve is destroyed. In Fig. 2 we highlight the region close to curve 1 (red curve) for $\varepsilon < \varepsilon_c$ (Fig. 2(a)) and for $\varepsilon = \varepsilon_c$ (Fig. 2(b)). It is possible to notice for $\varepsilon < \varepsilon_c$ the existence of other spanning curves close to curve 1. However, for $\varepsilon = \varepsilon_c$ many of these curves and also other structures are destroyed giving rise to chaos. Note that for $\varepsilon = \varepsilon_c$ curve 1 still exists, leading to believe that such a curve is actually quite robust.

In order to investigate in more detail the neighborhood of this curve, we apply again Slater's theorem, now for a region very close to the curve studied shown in Fig. 3. In this part of the analysis we did not choose the value of the rotation number, instead we did a sweep along the line $\phi = 3.0$, corresponding to the dashed magenta line in Fig. 3(a,b), and with a step in the variable V in the order of 10^{-6}. For each pair

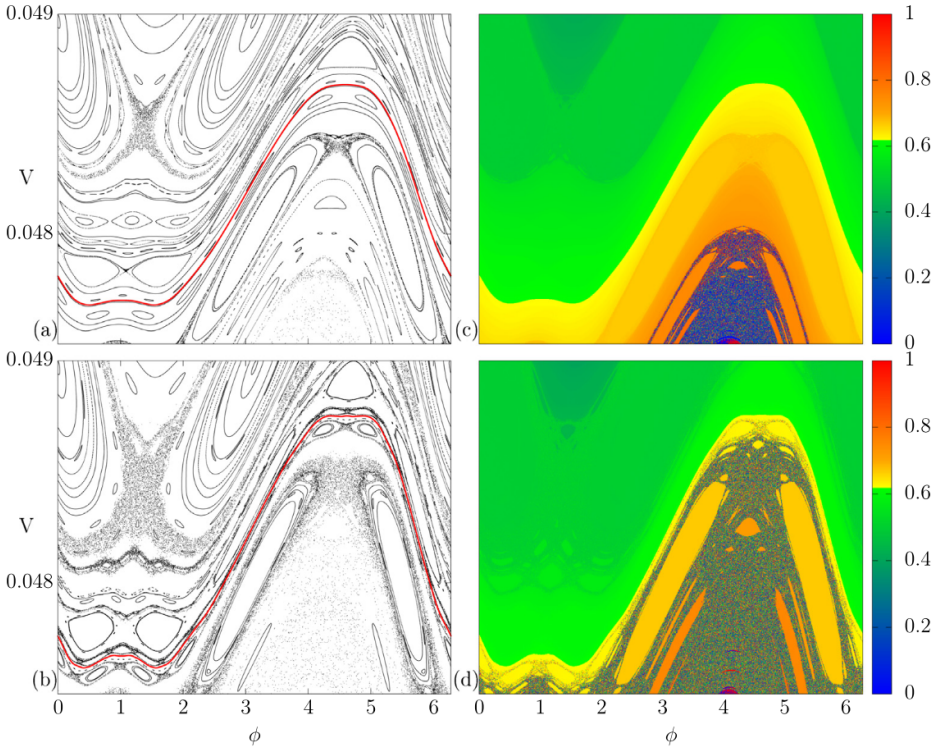

Fig. 2. Detail of the phase space in the vicinity of the curve 1 (red curve), (a) $\varepsilon = 5 \cdot 10^{-4}$ and (b) $\varepsilon = \varepsilon_c = 5.652 \cdot 10^{-4}$. (c, d) Same region as (a) and (b) where the colour scale corresponds to the decimal part of the rotation number. (For interpretation of the references to colour in this figure legend, the reader is referred to the web version of this article.)

(ϕ_0, V_0) we check if Slater's theorem was satisfied, that is, it has only 3 return times, the largest of which is equal to the sum of the other two. If so, according to the theorem, the pair (ϕ_0, V_0) belongs to a quasi-periodic orbit, which can be a spanning curve or, for example, an island. In Fig. 3(a), where $\varepsilon < \varepsilon_c$, the theorem was satisfied a few times and in these cases we highlighted in blue some of the curves that satisfied it. Doing the same procedure for $\varepsilon = \varepsilon_c$ (Fig. 3(b)) we found some islands that presented recurrence times according to Slater's theorem, which we highlight again in blue. However, we did not find other spanning curves in this region that met the theorem, only curve 1. This indicates that the curve studied is in a very thin and robust layer and that it is the most robust invariant spanning curve in the analyzed location or is very close to it. For $\varepsilon > \varepsilon_c$ this curve is also destroyed allowing chaos to advance. This critical value ε_c allows us to find a better approximation when we use Eq. (2), as can be seen in Fig. 1 where it is possible to notice that the blue dashed line representing the approximation is very close to the invariant spanning curve.

Extending Slater's theorem to other regions of the phase space, more precisely to regions of high energy, it was possible to find other curves that also satisfied Slater's theorem. All curves highlighted in Fig. 5 met the theorem. These curves have a rotation number equal to the golden

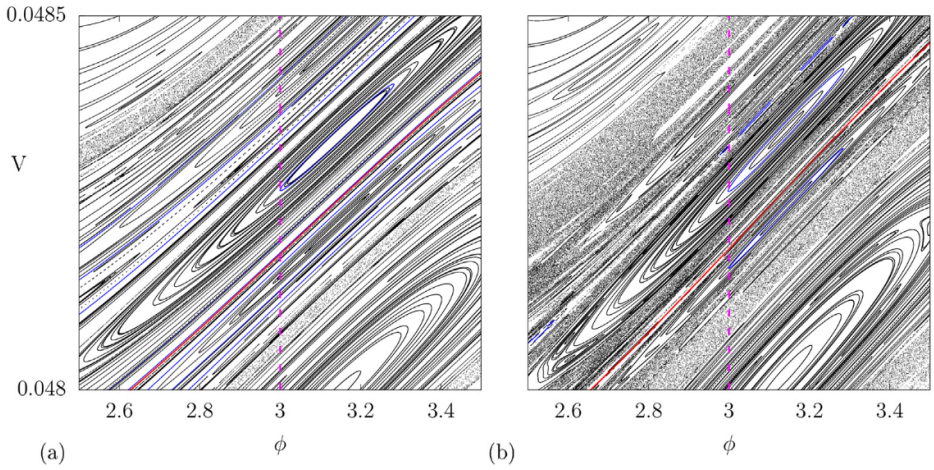

Fig. 3. Magnification of the phase space in the vicinity of the curve 1 (red curve). The blue curves satisfied Slater's theorem, (a) $\varepsilon = 5 \cdot 10^{-4}$ and (b) $\varepsilon = \varepsilon_c = 5.652 \cdot 10^{-4}$. (For interpretation of the references to colour in this figure legend, the reader is referred to the web version of this article.)

mean γ, or an integer shift of that value. Therefore, the recurrence times for these curves are consecutive numbers in the Fibonacci sequence. The Table 2 summarizes the position of each of these curves as well as the critical parameter found for each of them. The results presented in Table 2 allow us to see that the curves are consecutively destroyed, starting from the low energy curve (curve 1) to the highest energy curve (curve 6). This result was plotted in the graph of Fig. 4 and with a power-law fit we recovered the saturation exponent $\alpha = 1/2$ determined in Eq. (2).

With the theorem it is possible to analyze other curves with rotation numbers different from $\omega = [a_0; \overline{1}]$, such as curves with rotation number $\omega = [a_0; 2, \overline{1}]$. Curves with these rotation numbers have convergents $(\frac{p_n}{q_n})$ such that the sequence generated by q_n continues to satisfy the recurrence Eq. (4), now with $q_1 = 1$ and $q_2 = 2$. Thus, the return times for these curves are consecutive numbers from this new sequence. For example, the curve with rotation number $\omega = [a_0; 2, \overline{1}]$ is located in the vicinity of curve 1 and has return times $\Gamma_1 = 121393$, $\Gamma_2 = 196418$ and $\Gamma_3 = 317811$, with $\delta = 10^{-4}$ and step $\Delta V = 10^{-13}$ and $(\phi = 3.0, V_0 = 0.0496539561477)$. Regarding the critical parameter we find $\varepsilon_c = 0.00051$, which means that this curve is destroyed before curve 1 with $\omega = [a_0; \overline{1}]$.

In general, the sequences p_n and q_n satisfy the recurrences

$$p_{n+2} = a_{n+2}p_{n+1} + p_n, \tag{5}$$

$$q_{n+2} = a_{n+2}q_{n+1} + q_n, \tag{6}$$

for all $n \geqslant 0$, with $p_0 = a_0$, $p_1 = a_0a_1 + 1$, $q_0 = 1$ and $q_1 = a_1$. Furthermore, $p_{n+1}q_n - p_nq_{n+1} = (-1)^n$, for all $n \geqslant 0$. With these results it is possible to study other curves of the phase space, which have rotation number ω that generate in their convergent sequences of q_n different from the Fibonacci sequence. For, once the rotation number ω is known and consequently its expansion in continued fractions, the return times for this curve are consecutive numbers of this new sequence of q_n given by eq. (6). With this, the critical parameter for these curves can also be calculated and it is possible to predict the rupture of these curves. In this work, we focus on studying only the curves with noble rotation numbers, firstly because they are robust curves and also because of the practicality since the sequence generated by the q_n is a Fibonacci sequence for these cases.

4. Rotation numbers

The study of invariant curves in two-dimensional maps that conserve the area in phase space is closely linked to the concept of the rotation number. An orbit $\{(\phi_t, V_t) : t \in \mathbb{Z}\}$ of mapping 1, has rotation number ω if the limit

$$\omega = \lim_{N\to\infty} \frac{1}{N} \sum_{t=0}^{N-1} \Omega(V_t) \tag{7}$$

exists. In Eq. (7), $\sum_{t=1}^{N} \Omega(V_t) = \phi_N - \phi_0$ and N corresponds to the number of iterations.

Table 3 presents the values of the rotation numbers calculated from Eq. (7) for each of the curves highlighted in Fig. 5. It is important to note

Table 2
Critical ε value for each of the curves in Fig. 5.

	ε_c	V
Curve 1	0.0005652	0.04818861506
Curve 2	0.0007850	0.05678598945
Curve 3	0.0011640	0.06911780565
Curve 4	0.0019000	0.08829265188
Curve 5	0.0036478	0.12219771899
Curve 6	0.0096495	0.19841892983

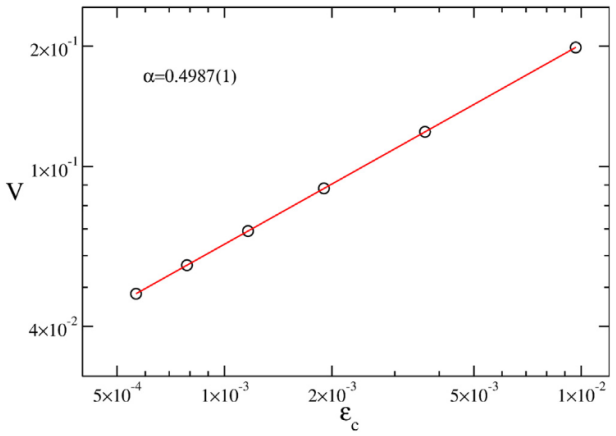

Fig. 4. Plot of V *vs.* ε_c. A power-law fit gives $\alpha = 0.4987(1)$.

that for each of these curves the rotation numbers differ only in the whole part, its decimal part being equal to the golden mean γ, as can be seen in the continued fraction expansion in the last column of the table. Furthermore, the rotation numbers found for each of the curves are noble numbers, as proposed by Fox [37]. Particularly, the noble numbers form a set of quadratic irrationals, that is, they can be written in the form: $(P \pm \sqrt{M})/S$, where $P, M, S \in \mathbb{Z}$, like those shown in the third column of the Table 3. Moreover, the invariant curves located in the low-energy region have a higher rotation number than those located in the high-energy region, that is, for higher values of V. More precisely, for the curves found from Slater's Theorem, their rotation numbers decrease by one unit as we take a curve higher up. It even reaches the last curve (curve 6) with rotation number $\omega = \frac{1+\sqrt{5}}{2} = 1.618033\ldots$.

As highlighted above, in Fig. 2 we show the dynamics in the neighborhood of the curve 1 (red curve) with the phase space constructed for the parameter before the criticality $\varepsilon < \varepsilon_c$ (Fig. 2(a)) and for $\varepsilon = \varepsilon_c$ (Fig. 2(b)). In Fig. 2(c,b) we have the same region of the phase space, but the colour scale is given by the decimal part of the rotation number, calculated from Eq. (7). In Fig. 2(c), $\varepsilon = 5 \cdot 10^{-4}$, it is possible to notice two distinct regions, one in shades of green with $\omega < 0.6180339\ldots$ and the other in shades of yellow with $\omega > 0.6180339\ldots$. Moreover, chaotic dynamics does not lead to the convergence of the rotation number. The boundary between these two regions corresponds to the invariant spanning curve. Therefore, the orbits above the curve have a lower number of rotation than those below the curve. In Fig. 2(d), with $\varepsilon = 5.652 \cdot 10^{-4}$, we can see an advance in the chaotic regions caused by the increase in the parameter ε. However, the curve still exists for this parameter value and it acts as a barrier preventing chaos from entering into the region above the curve. This effect was also observed for the other five curves in Fig. 5 found using Slater's theorem. This evidence reinforces the idea that invariant spanning curves with rotation number $\omega = [a_0; \overline{1}]$ are quite robust, at least in the layer where each one of them persists.

Table 3
Rotation numbers found for each of curves in the Fig. 5. Column 1 identifies the curve. Column 2 furnishes the rotation number obtained from Eq. (7), which numerical value is very close to the analytical result shown in column 3 foresaw from the expansion displayed in column 4.

Curve 1	6.6180339815	[6;1,1,1,1,1,1,...]
Curve 2	5.6180339845	[5;1,1,1,1,1,1,...]
Curve 3	4.6180339989	[4;1,1,1,1,1,1,...]
Curve 4	3.6180339829	[3;1,1,1,1,1,1,...]
Curve 5	2.6180339686	[2;1,1,1,1,1,1,...]
Curve 6	1.6180339660	[1;1,1,1,1,1,1,...]

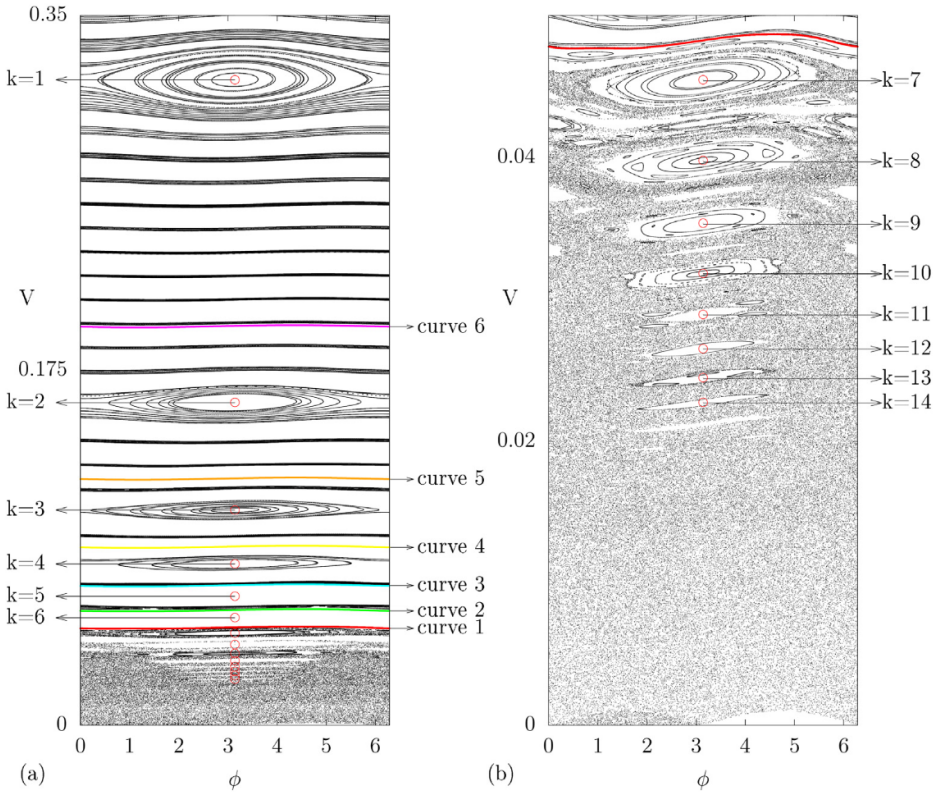

Fig. 5. (a) Phase space for the Fermi-Ulam Model with $\varepsilon = 5 \cdot 10^{-4}$. All invariant curves found from Slater's Theorem are highlighted. Elliptical fixed points are indicated by red circles. (b) Magnification of the region below the first invariant spanning curve (red curve). (For interpretation of the references to colour in this figure legend, the reader is referred to the web version of this article.)

In order to understand the dynamics close to the invariant spanning curves, we calculated the rotation number profile in the vicinity of curve 1. In Fig. 6(a) we highlight the region close to (red curve), the rotation number was calculated along the dashed blue line and its fractional part represented in Fig. 6(b). The rotation number profile has a fractal characteristic, very similar to the "Devil's Staircase" [39]. It is known that in area-preserving maps, the area under an invariant set as a function of frequency is a Devil's staircase [40]. Our result is analogous to the presentation in [40], however, in our case the action V as a function of the rotation number ω that generated a staircase.

The first analytic theory for the Devil's staircase was described by Aubry [41,42] in an extended Frenkel-Kontorova model as a

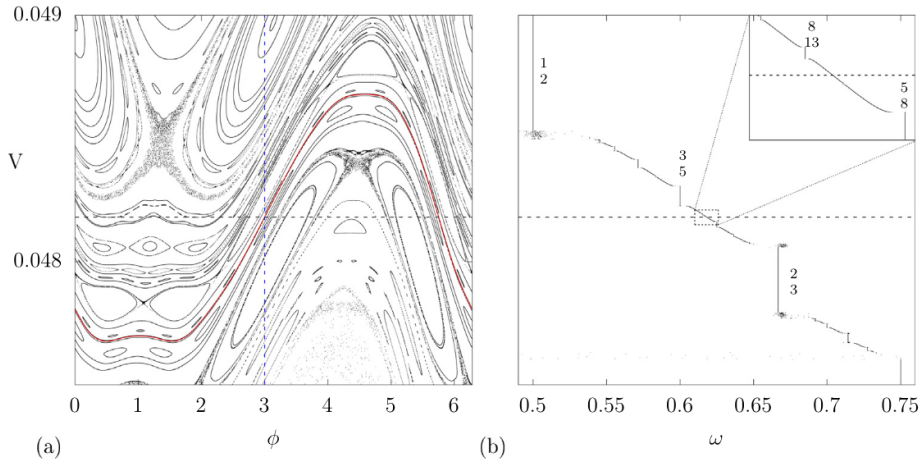

Fig. 6. (a) Detail of the phase space in the vicinity of the first invariant spanning curve (red curve). (b) Rotation number profile calculated along the blue line highlighted in (a), some rotation number values are indicated in the figure and an enlargement is made in the region near the invariant curve. (For interpretation of the references to colour in this figure legend, the reader is referred to the web version of this article.)

consequence of the analyticity break transition. This theory did not involve any numerical calculation. Aubry in [43] described two exact models that exhibit a Devil's staircase. The first was a discrete Frenkel-Kontorova model and the second was an Ising chain over an external magnetic field. Additionally, this Devil's staircase structure can be found in a variety of physical situations.

Still in Fig. 6(b), we indicate some values of the rotation number which form the Farey sequence [44], that is, if $\frac{a}{b}$ and $\frac{c}{d}$ are neighbors, then the next term that appears between them according to the Farey order is $\frac{a+c}{b+d}$, so, the term between $\frac{1}{2}$ and $\frac{2}{3}$ is . Furthermore, the terms of this sequence are Fibonacci sequence numbers as well as the terms of the continued fraction expansion in the rotation number ω of the curve.

5. Discussions and conclusions

We used Slater's theorem to determine the break-up of invariant curves in the phase space of the Fermi-Ulam model and the associated critical parameters. Such theorem relates the recurrence times and the continued fractional expansion of the curve rotation number. These recurrence times depend on the size of the recurrence interval δ, which gets larger and larger as we decrease the δ value. Longer times represent a better approximation of the irrational rotation number by continued fractions since these times are denominators in the expansion. However, it is necessary to be careful when choosing δ, avoiding the need for a very large number of iterations and, consequently, high computational cost.

Through Slater's theorem, we were able to find the position of a family of locally robust invariant spanning curves. The use of the theorem allowed us to study the criticality for each of these curves. We determined the parameter ε_c related to each curve and thus we were able to predict their breakage. These curves are consecutively destroyed from bottom to top in phase space, as we increase the value of the ε parameter. With curve 1 (Fig. 5) being the first to be destroyed, with $\varepsilon_c = 0.0005652$ and curve 6 (Fig. 5) the last, with $\varepsilon_c = 0.0096495$.

An analysis near the first invariant spanning curve (curve 1) revealed that as we increase the value of the parameter ε, the periodic structures and invariant curves close to the curve are destroyed, as predicted by the KAM theory. Finally, for $\varepsilon_c = 0.0005652$, in this region, the only invariant spanning curve that still survives is curve 1. Such behavior was observed for all other curves in Fig. 5 found from Slater's theorem. Although we do not yet have a mathematical procedure to prove that the highlighted invariant curves are the most locally robust, we found strong numerical evidence that they belong to a robust thin layer and that such curves are more robust in the analyzed region.

Furthermore, the rotation number for these curves decreases as the curve is located further up in the phase space. The rotation number profile in the vicinity of the curves presented a structure similar to a "Devil's Staircase". The organization of the rotation numbers in this structure follows a Farey tree and the terms that belong to the Fibonacci sequence converge to the position of the invariant spanning curve in the region.

CRediT authorship contribution statement

Joelson D.V. Hermes: Conceptualization, Methodology, Software, Formal analysis, Writing – original draft. **Marcelo A. dos Reis:** Software, Validation, Formal analysis, Writing – review & editing. **Iberê L. Caldas:** Validation, Formal analysis, Writing – review & editing, Supervision. **Edson D. Leonel:** Validation, Formal analysis, Writing – review & editing, Supervision.

Data availability

No data was used for the research described in the article.

Declaration of competing interest

The authors declare that they have no known competing financial interests or personal relationships that could have appeared to influence the work reported in this paper.

Acknowledgements

We would like to acknowledge financial support from the Brazilian agencies: São Paulo Research Foundation (FAPESP) - Grant No. 2018-03211-6 and CNPq-Grant Nos. 302665-2017-0 and 407299-2018-1. JDVH thanks Federal Institute of Education, Science and Technology of South of Minas Gerais - IFSULDEMINAS.

References

[1] Luna-Acosta G, Méndez-Bermúdez J, Šeba P, Pichugin K. Classical versus quantum structure of the scattering probability matrix: chaotic waveguides. Phys Rev E. 2002.;65(4):046605.
[2] Zaslavsky GM. Chaos, fractional kinetics, and anomalous transport. Phys Rep. 2002; 371(6):461–580.
[3] Szezech Jr J, Caldas I, Lopes S, Viana R, Morrison P. Transport properties in nontwist area-preserving maps. Chaos. 2009.;19(4):043108.
[4] Soskin S, Mannella R, Yevtushenko O. Matching of separatrix map and resonant dynamics, with application to global chaos onset between separatrices. Phys Rev E. 2008.;77(3):036221.
[5] del Castillo-Negrete D. Chaotic transport in zonal flows in analogous geophysical and plasma systems. Phys Plasmas. 2000;7(5):1702–11.
[6] Portela J, Caldas I, Viana R. Tokamak magnetic field lines described by simple maps. Eur Phys J Spec Top. 2008;165(1):195–210.
[7] Morrison P. Magnetic field lines, hamiltonian dynamics, and nontwist systems. Phys Plasmas. 2000;7(6):2279–89.
[8] Stöckmann H-J, Persson E, Kim Y-H, Barth M, Kuhl U, Rotter I. Effective hamiltonian for a microwave billiard with attached waveguide. Phys Rev E. 2002.;65(6):066211.
[9] Leonel ED. Corrugated waveguide under scaling investigation. Phys Rev Lett. 2007.; 98(11):114102.
[10] Karlis A, Diakonos F, Constantoudis V. A consistent approach for the treatment of fermi acceleration in time-dependent billiards. Chaos. 2012.;22(2):026120.
[11] Leonel ED, Oliveira DF, Loskutov A. Fermi acceleration and scaling properties of a time dependent oval billiard. Chaos. 2009.;19(3):033142.
[12] Mei S, Shen T, Hu W, Lu Q, Sun L. Robust h control of a hamiltonian system with uncertainty and its application to a multi-machine power system. IEE Proc Control Theory Appl. 2005;152(2):202–10.
[13] Mei F, Wu H. Generalized hamilton system and gradient system. Sci Sin Phys Mech Astron. 2013;43(4):538–40.
[14] Chirikov BV, Zaslavsky GM. Stochastic instability of nonlinear oscillations. Sov Phys Usp. 1972;14(5):549–672.
[15] Kolmogorov AN. On conservation of conditionally periodic motions for a small change in hamilton's function. Dokl Akad Nauk SSSR. 1954;98:527–30.
[16] Arnold VI. Proof of a theorem of an kolmogorov on the preservation of conditionally periodic motions under a small perturbation of the hamiltonian, uspehi mat. Nauk. 1963;18(5):113.
[17] Möser J. On invariant curves of area-preserving mappings of an annulus. Nachr Akad Wiss Göttingen, II. 1962:1–20.
[18] Meiss J. Symplectic maps, variational principles, and transport. Rev Mod Phys. 1992; 64(3):795.
[19] Fermi E. On the origin of the cosmic radiation. Phys Rev. 1949;75:1169–74.
[20] Ulam SM. On some statistical properties of dynamical systems. Contributions to astronomy, meteorology, and physics. University of California Press; 2020. p. 315–20.
[21] Lieberman MA, Lichtenberg AJ. Stochastic and adiabatic behavior of particles accelerated by periodic forces. Phys Rev A. 1972;5(4):1852.
[22] Pustyl'nikov L. Existence of invariant curves for maps close to degenerate maps, and a solution of the fermi-ulam problem. Sbornik: Mathematics. 1995;82(1):231.
[23] Pustyl'nikov LD. On the fermi–ulam model. Dokl Akad Nauk. 1987;292:549–53. Russian Academy of Sciences.
[24] Slater NB. The distribution of the integers n for which {n}¡. Math Proc Camb Philos Soc. 1950;46:525–34. Cambridge University Press.
[25] Lichtenberg AJ, Lieberman MA. Regular and chaotic dynamics. Appl Math Sci. 1992; 38:49. Springer-Verlag.
[26] Karlis AK, Papachristou PK, Diakonos FK, Constantoudis V, Schmelcher P. Hyperacceleration in a stochastic fermi-ulam model. Phys Rev Lett. 2006.;97 (19):194102.
[27] Leonel ED, da Silva JKL, Kamphorst SO. On the dynamical properties of a fermi accelerator model. Physica A. 2004;331(3–4):435–47.
[28] Chirikov BV. A universal instability of many-dimensional oscillator systems. Phys Rep. 1979;52(5):263–379.
[29] Leonel ED, McClintock PV, Da Silva JKL. Fermi-ulam accelerator model under scaling analysis. Phys Rev Lett. 2004.;93(1):014101.
[30] Leonel ED. Invariância de Escala em Sistemas Dinâmicos Não Lineares. 1st Edition. Blucher; 2019.

[31] MacKay RS, Percival IC. Converse kam: theory and practice. Commun Math Phys. 1985;98(4):469–512.
[32] Laskar J, Froeschlé C, Celletti A. The measure of chaos by the numerical analysis of the fundamental frequencies. Application to the standard mapping. Physica D. 1992;56(2–3):253–69.
[33] Lan Y, Chandre C, Cvitanović P. Newton's descent method for the determination of invariant tori. Phys Rev E. 2006.;74(4):046206.
[34] Greene JM. A method for determining a stochastic transition. J Math Phys. 1979;20 (6):1183–201.
[35] Altmann E, Cristadoro G, Pazó D. Nontwist non-hamiltonian systems. Phys Rev E. 2006.;73(5):056201.
[36] Abud CV, Caldas IL. On slater's criterion for the breakup of invariant curves. Physica D. 2015;308:34–9.
[37] Fox AM, Meiss JD. Critical invariant circles in asymmetric and multiharmonic generalized standard maps. Commun Nonlinear Sci Numer Simul. 2014;19(4):1004–26.
[38] MacKay R, Stark J. Locally most robust circles and boundary circles for area-preserving maps. Nonlinearity. 1992;5(4):867.
[39] Schuster HG, Just W. Deterministic chaos: an introduction. John Wiley Sons; 2006.
[40] Chen Q. Area as a devil's staircase in twist maps. Phys Lett A. 1987;123(9):444–50.
[41] Aubry S. Defectibility and frustration in incommensurate structures: the devil's stair case transformation. Ferroelectrics. 1980;24(1):53–60.
[42] Aubry S. The riemann problem, complete integrability and arithmetic applications. Lect Notes Math. 1980.;925.
[43] Aubry S. Exact models with a complete devil's staircase. J Phys C Solid State Phys. 1983;16(13):2497.
[44] Devaney RL. The mandelbrot set, the farey tree, and the fibonacci sequence. Am Math Mon. 1999;106(4):289–302.